PERGAMON

Computers & Geosciences 27 (2001) 901–912

COMPUTERS & GEOSCIENCES

A predictive GIS model for mapping potential gold and base metal mineralization in Takab area, Iran

H.H. Asadi[a,b,*], M. Hale[b]

[a] *Ministry of Culture and Higher Education, Dr. Beheshti Avenue, Shahid Sabounchi Cross, Tehran, Iran*
[b] *International Institute for Aerospace Survey and Earth Sciences (ITC), Kanaalweg 3, 2628 EB, Delft, Netherlands*

Received 1 January 1999; accepted 14 January 2000

Abstract

The 1785 km^2 Takab area of northwest Iran is a region of high mineral potential but difficult access for which an innovative exploration approach is required. Interpretation of aeromagnetic, Landsat TM, geological and mineral occurrence data are used to recognize a combination of mapped geological features, spectral characteristics, and magnetic signatures that could be associated with epithermal gold, arsenic, antimony, and base metal deposits near Takab. Geological data such as permeable, reactive host rocks, surface igneous rocks, and structures are integrated with interpretations of remotely sensed data of hydrothermal alteration and subsurface igneous heat sources. Four binary maps representing diagnostic deposit recognition criteria were combined in a weights-of-evidence model, which uses the spatial distribution of 19 known mineral occurrences to calculate a final map of further gold and base metal potential in the Takab area. © 2001 Published by Elsevier Science Ltd.

Keywords: Sediment-hosted gold deposits; Hydrothermal alteration mapping; Structural mapping; Magnetic signatures; Spatial modelling; Weights-of-evidence analysis

1. Introduction

The Takab area is a sparsely vegetated, semi-arid, mountainous region of 1785 km^2, located to the north of the town of Takab, northwest Iran (Fig. 1). It is one of the most important gold-mineralized regions of Iran and includes an active arsenic mine (Zarshuran), two known gold deposits (Zarshuran and Aghdarreh), the largest lead–zinc mine in Iran (Anguran), another smaller lead–zinc mine (Alamkandy), a large copper mine (Baiche-Bagh) and evidence of several ancient mining activities for gold, arsenic, antimony and base metals.

This paper reviews the geologic setting and mineralization of the Takab area and outlines the recognition criteria for epithermal gold and base metal mineralizations. The application of spectral and geophysical remote-sensing tools for mapping hydrothermal alteration, igneous rocks, and structures that could be spatially associated with the known mineral deposits are then demonstrated. Based on weights-of-evidence analysis of geologic, spectral, and magnetic data representative of the deposit recognition criteria, a predictive geographic information system (GIS) model is constructed to locate areas of interest for future gold and base metal exploration.

2. Geologic background

The Takab area lies at the boundary of the Urumieh-Dokhtar volcanic arc and the Sanandag-Sirjan volcano-sedimentary zone, both of which extend over 2000 km in a NW–SE direction parallel to the Zagros thrust fault. Alavi (1993) has interpreted this boundary as the suture zone between the Afro-Arabian and Iranian plates. It is

*Correspondence address: International Institute for Aerospace Survey and Earth Sciences, P.O. Box 6, 7500 Enschede, Netherlands.

E-mail address: hale@itc.nl (M. Hale).

0098-3004/01/$ - see front matter © 2001 Published by Elsevier Science Ltd.
PII: S0098-3004(00)00130-8

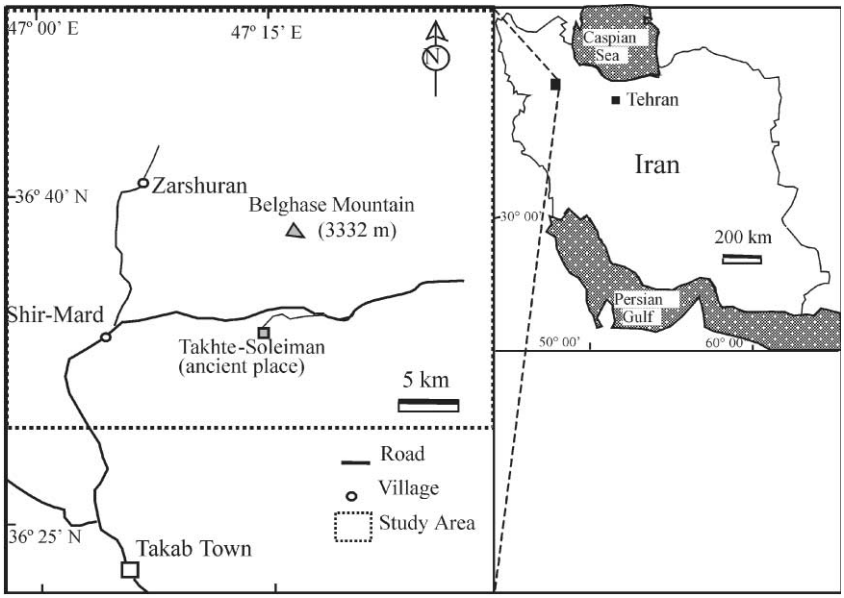

Fig. 1. Location map of Takab area.

characterized by a series of structural depressions, sheared and mylonitized rock sequences, and high-angle, northeast-dipping shear planes. The widespread Tertiary volcanism of the Urumieh-Dokhtar arc is attributed by Berberian and King (1981) to northeast-dipping subduction of the Arabian plate under the Iranian plate along the Zagros thrust fault which is located 150–200 km west of Alavi's suture zone.

The area has experienced repeated cycles of orogenic activity, including structural uplift, sedimentation, magmatism and metamorphism (Alavi et al., 1982). The geological formations mostly comprise Precambrian metamorphics, Tertiary volcanics (with subordinate granitoids and sediments) and Quaternary sediments. Tertiary volcano–plutonic rocks underlie about 30% of the area and the volcanics are partially altered throughout the area. A major northwest–southeast trending fault puts the Precambrian metamorphics in juxtaposition with the Tertiary rocks in the middle of the area (Fig. 2).

3. Mineralization

The known gold, arsenic, antimony and base metal mineralizations are mainly epithermal in origin and are hosted by jasperoid, black shale, carbonates and partially altered andesite. Those deposits hosted by sediments are usually found a short distance from volcano–plutonic rocks.

Zarshuran, the largest gold deposit of the area, is a disseminated gold deposit hosted by Precambrian black shale and carbonates, which have been intruded by a weakly mineralized, highly altered granitoid. This intrusion fractured the host formation and provided a favorable site for mineralizing hydrothermal solutions. Decalcification, sericitization and kaolinitization are the principal alterations. The mineralization is mainly controlled by NE–SW and E–W trending high angle faults intersecting the southwest limb of a NW–SE plunging anticline. Zarshuran in many respects is very similar to the Carlin-type sediment-hosted gold deposits of the western United States (Asadi et al., 1999a). The gold mainly occurs as invisible gold associated with arsenic-bearing pyrite and sphalerite; visible gold is rare and occurs in orpiment and silica (Asadi et al., 1999b). Compared to the Carlin-type deposits, the presence of higher tellurium concentrations in the ore and close association with igneous rocks at Zarshuran indicate a larger than typical magmatic component in the mineralizing hydrothermal solutions (Asadi and Hale, 1999b).

Aghdarreh, the second biggest gold deposit in the Takab area, occurs in a domed, locally thickened Oligo-Miocene limestone. It comprises two separate mineralized areas about 1.5 km apart, prominently marked by the occurrence of jasperoid veins and lenses trending NE–SW and NNE–SSW. Tuffaceous volcanic lenses are present at the top of the limestone, and may be related to the volcanic rocks located 4–5 km to the northeast (toward Zarshuran). The richest mineralization occurs in jasperoid lenses in the upper part of the limestone and in underlying horizons, conformable with the limestone bedding, rich in iron and manganese oxides. The jasperoids and the iron–manganese oxide horizons are

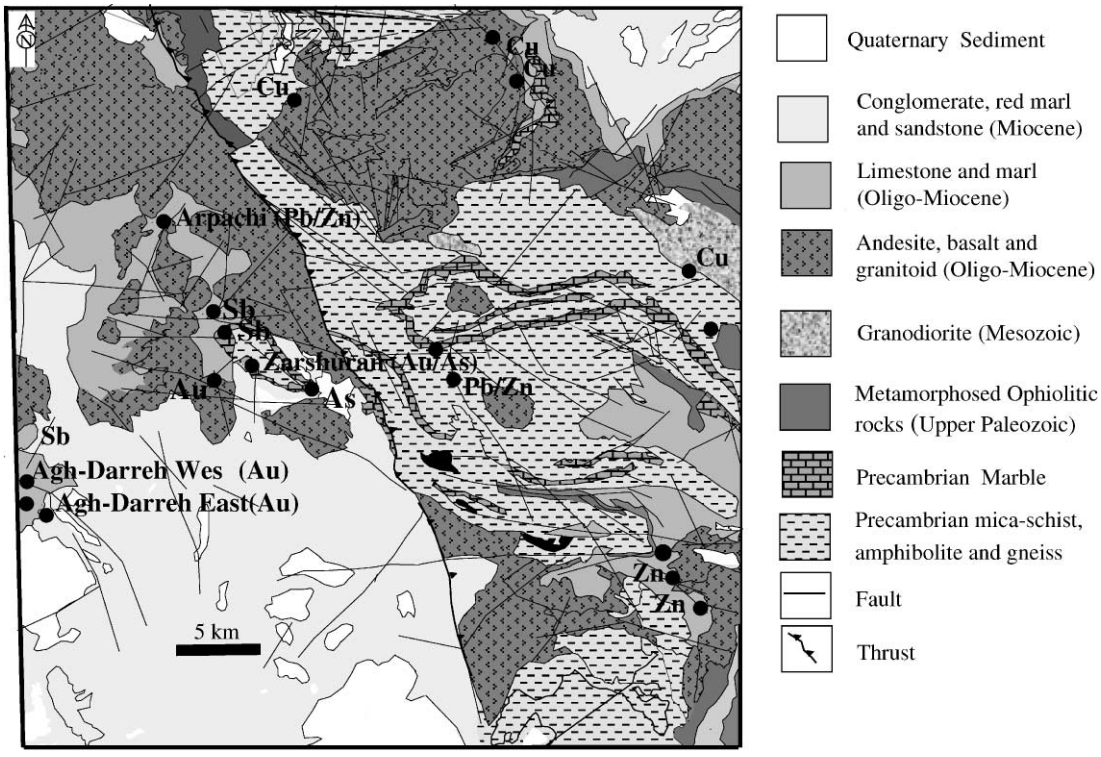

Fig. 2. Geological and mineral occurrence map of Takab area.

enriched to economic proportions in gold with accompanying arsenic, antimony, zinc, lead, silver and barium. According to Daliran et al. (1999), the mineralization is epithermal in origin.

There are also a number of less significant arsenic, antimony and gold prospects in the vicinity of Zarshuran and Aghdarreh. Arsenic is being worked on a small scale from NE–SW trending silicified veins and lenses in the Zarshuran Precambrian black shale unit. At Baldir-Ghanee, about 2 km northwest of Zarshuran, there are traces of antimony mineralization. The mineralization is identified by massive silicification in Oligo-Miocene limestone and shale, and is closely associated with Miocene volcanics. At Bighair-Bolaghi, located 1 km north of Baldir-Ghanee, there are several indications of antimony mineralization in the carbonate rocks, which are intruded by altered Oligo-Miocene andesite dykes (Karimi, 1992). There are several old workings at Chaldaghi and Kalaki, a few km to the west of Zarshuran, where small mineralized quartz veins occur at the top of Miocene volcanic sequences. Mohajer et al. (1989) reported up to 5.4 ppm gold from a quartz vein at Kalaki. A small abandoned antimony mine is located about 2 km to the north of Aghdarreh. The stibnite mineralization at this mine is hosted by ferruginous carbonate, marl and black shale and appears to be controlled by NE–SW trending faults. Highly altered granitoid rocks are widespread about 2 km to the north of the mineralized area.

The Anguran lead–zinc mine is the largest mine in the area. The ore body is hosted by fractured, Oligo-Miocene calcareous rocks, which overlie Precambrian metamorphic and metavolcanic rocks. The dominant structure of the deposit is a ENE–SSW trending anticline intersected by NW–SE and E–W trending faults which control the mineralization. Ore minerals are mainly sphalerite and galena in the lower part of the ore body and smithsonite, hemimorphite, zincite, sericite, and iron oxides in the upper part. Oligo-Miocene andesitic rocks are located in the immediate vicinity of this deposit.

There are additional lead and zinc occurrences at Alamkandy and Arpachi. Mineralization at Alamkandy is hosted by ferruginous carbonates located along their contact with Precambrian metamorphic rocks. The mineralized rocks extend in a NW–SE direction. Vein-type mineralization at Arpachi is hosted by Oligo-Miocene carbonates located close to an altered Miocene andesite. The mineralization is controlled by NE–SW trending faults.

Vein copper mineralization occurs in fractured and faulted zones in altered Oligo-Miocene andesite at Baiche-Bagh. The main NNE–SSW structural trend controls the mineralization in this area. Silica, kaolinite,

sericite and limonite are the main alteration products. The silicifed veins, 0.5–1.5 m thick and up to 2 km long, commonly contain chalcopyrite, tetrahedrite, arsenopyrite, pyrite, sphalerite, galena, and bismuthinite. Bulk chemical analyses of a few samples indicated high gold and silver concentrations (Zanjani, 1945) and Bariand (1962) reported the presence of native gold associated with arsenopyrite.

There are further copper occurrences, most of them old workings within the altered Oligo-Miocene andesite in the northwest of the Takab area. Mineralization in these occurrences is mainly controlled by E–W and NE–SW trending structures.

4. Recognition criteria

Sediment-hosted epithermal mineralizations are scattered throughout the Takab area. Their characteristic recognition criteria appear to be: (1) host-rock lithology; (2) association with volcano–plutonic rocks; (3) hydrothermal alteration; and (4) geologic structures. These criteria are those also exhibited by Carlin-type deposits. According to Bagby and Berger (1985), high permeability and chemical reactivity in the host formations provide favorable conditions for the precipitation from mineralizing hydrothermal solutions of Carlin-type gold deposits. In the Takab area, these conditions occur in the black shales, carbonates and marls, which together host most of the known mineralization in the area.

Bagby and Berger (1985) point out that nearly all of the Carlin-type gold deposits in Nevada are spatially associated with intermediate to acid igneous rocks that are either exposed at surface or concealed at a shallow depth. There are partially-altered andesites and highly altered granitoid rocks in the immediate vicinity of the Zarshuran gold deposit as well as near most of the other hydrothermal gold, arsenic, antimony and base metal mineralizations in the area. Asadi and Hale (1999a) attribute high-amplitude aeromagnetic anomalies within the Takab area to high magnetic susceptibility igneous rocks. The highest anomalies are located in the central part of the area and coincide with the location of the Zarshuran deposit and its surroundings. At a distance of 2–3 km from Zarshuran these anomalies can be ascribed to widespread outcrops of Oligo-Miocene volcanics, some of which are mineralized. In the immediate vicinity of Zarshuran, however, surface exposures are Precambrian and Oligo-Miocene sediments, but high-amplitude magnetic anomalies here suggest the presence of igneous intrusive rocks beneath the Zarshuran deposit and other nearby arsenic and antimony mineralizations. Oligo-Miocene volcanic rocks and granitoids appear to have provided the main heat sources for the hydrothermal systems resonsible for gold, arsenic, antimony, and base metal mineralization, and have also been a source for gold-bearing hydrothermal solutions (Asadi and Hale, 1999b). Some igneous bodies in the area have been altered and mineralized, indicating that the hydrothermal systems post-dated associated magmatic events.

The presence of hydrothermally altered zones is an important guide to epithermal deposits of the area. Two types of hydrothermal alteration, argillic and iron oxide, are associated with most of the known mineral deposits of the area (Asadi and Hale, 1999b) and each provides an important deposit recognition criterion. For example, the Zarshuran gold deposit is characterized by argillic hydrothermal alteration, while the Aghdarreh gold deposit is characterized by iron oxide hydrothermal alteration.

Structures, and particularly structural intersections, are also important for controlling magmatism, hydrothermal fluid flow, and mineral deposition in the Takab area. At the district and deposit scale the NE–SW, NW–SE and E–W trending faults and their intersections appear to control the mineralization in most of the known deposits of the area. Asadi et al. (1998) show that most of the known mineral deposits of the area are located in a 500 m buffer zone from the NE–SW and E–W trending lineaments interpreted from Landsat TM data.

5. Input maps

A digital data base of known mineral deposits and likely controls on mineralization of the Takab area was established. Most of the known mineral deposits of the area were digitized from the mineral occurrence map of the Takab–Shahin–Dez quadrangle (1 : 250,000 scale) published by Ministry of Mines and Metals of Iran (1994). Some of the small occurrences were digitized from 1 : 100,000 scale geological map of the Takab area published by Geological Survey of Iran (1998), and also from the district scale geological maps of Zarshuran and Aghdarreh mining area (Samimi, 1992; Mineral Export Company, 1995). The data base consists of 19 mineral occurrences extracted from these maps. The controls on mineralization consist of (1) suitable host lithologies, digitized from the 1 : 100,000 scale geological map of the area published by the Geological Survey of Iran (1998); (2) volcano–plutonic heat sources, digitized from the same geological map and interpreted from the analytical signal of the total intensity magnetic field image; (3) hydrothermal alteration zones interpreted from the selected Landsat TM bands and reduction to the pole of aeromagnetic data; and (4) lineaments digitized from the 1 : 100,000 geological map and derived from the shaded relief total intensity magnetic field image.

5.1. Map of favorable host lithologies

In the Takab area, most of the gold and base metal mineralization, in particular in the Zarshuran and Aghdarreh gold deposits and the Anguran lead-zinc deposit, are hosted by chemically-reactive and permeable sedimentary formations. These include Precambrian black shales and carbonates, fractured Oligo-Miocene calcareous shales, karsted limestones, ferruginous carbonates and marls. The mapped outlines of these units were digitized from the 1 : 100,000 scale geological map of the area and converted to raster format.

5.2. Map of heat sources

Heat sources for hydrothermal systems include outcropping and concealed Oligo-Miocene volcano–plutonic rocks (i.e., andesites and granitoid intrusions). These outcrop over 21.4% of the Takab area. Still more are expected to lie beneath the surface. High-resolution aeromagnetic data of the Takab area were used to remap the main geological units and infer the subsurface geology.

Aeromagnetic data were retrieved from nine analog total magnetic intensity contour maps (1 : 50,000 scale) produced as part of an aeromagnetic survey of the Takab–Shahin–Dez Quadrangle carried out in 1978 by Prakla-Seismos GMBH of Germany. The flight lines were oriented N–S with a spacing of 500 m and a nominal terrain clearance of 120 m. The procedure described by Paterson and Reeves (1985) was used to perform analytic signal analysis of the total magnetic intensity in order to identify anomalously high magnetic fields associated with high magnetic susceptibility igneous rocks, both at surface and at depth.

Fig. 3 is the shaded relief color analytical signal of total magnetic intensity map of the Zarshuran area in which anomalously high-amplitude analytic signal anomalies appear as purple shades. The highest anomalies are located in the central part of the area and coincide with the Zarshuran deposit and its surroundings. At a distance of 2–3 km from Zarshuran these anomalies can be ascribed to widespread outcrops of Tertiary volcanics. Most of the igneous rocks interpreted from the analytic signal image are high-confidence subsurface extensions of exposed Tertiary andesites. The Tertiary andesites are partially mineralized and spatially associated with most of the known mineral deposits in the area. The mapped subsurface igneous rocks represent 6.8% of the study area.

5.3. Map of hydrothermal alteration

Asadi and Hale (1999a) applied a principal components transformation to the selected reflective Landsat-

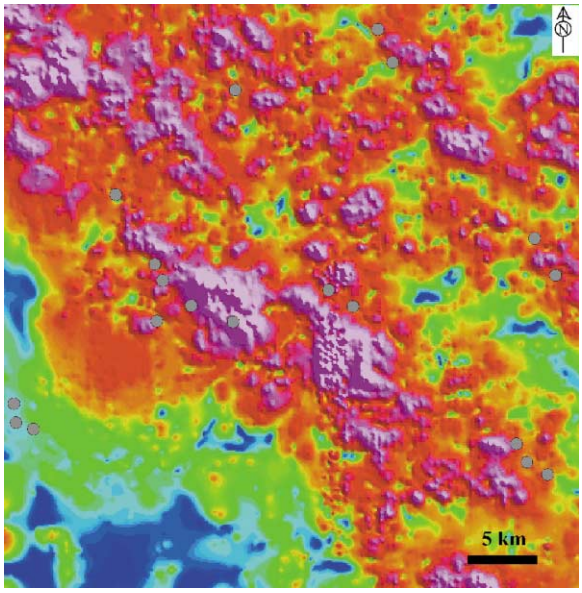

Fig. 3. Analytical signal map of total magnetic intensity showing high analytical signal as purple shades.

TM bands of the Takab area and mapped iron oxides and hydroxyl-bearing minerals, some of which result from hydrothermal alteration associated with known epithermal mineralizations in the area. Ground truthing and spatial analysis indicated that most of the mapped hydroxyl zones are spatially associated with the igneous heat sources and controlled by the linear structures of the area. They are mainly argillic hydrothermal alteration which characterizes many of the known mineral deposits.

Some of the mapped iron oxide zones are located in the southern part of the area, where there is no evidence of volcanic activity to form hydrothermal alteration. These iron oxides in the south, associated with a Miocene red sandstone formation, are attributed to surface weathering.

In addition, reduction to the pole of the total magnetic intensity data was used by Asadi and Hale (1999a) to map iron oxide hydrothermal alteration zones associated with epithermal mineralization of the area. They argued that zones of weak magnetic responses highlighted by the reduction to the pole image are likely to arise from the demagnetization of magnetite in contact with hydrothermal fluids, yielding epigenetic hematite and limonite.

5.4. Map of structures

Faults trending NE–SW, E–W and NW–SE, which have spatial association with known mineralization in the area, were digitized from the 1 : 100,000 geologic map of the area. In addition, shaded relief total

magnetic intensity data of the area was used to map those structures (i.e., surface and subsurface faults) that were not recorded on the geological map. Successful representation of lineament features in shaded relief depends upon the choice of illumination azimuth (preferably perpendicular to the linear features), illumination angle above the horizon, and exaggeration of vertical scale. For the Takab area, two different illumination angles were chosen to map the structures trending in different directions. A shaded relief map of total magnetic intensity with artificial illumination of azimuth of 45°, an inclination of 45°, and a scale factor of 0.35 highlights the major structural features oriented in a NW–SE direction parallel to the Zagros thrust. A map with azimuth 315°, inclination 45° and scale factor 0.35 shows lineaments perpendicular to the major structures (Fig. 4). Many of the known mineral deposits of the area lie on or close to these lineaments.

6. Weights-of-evidence method

Bonham-Carter et al. (1989) and Bonham-Carter (1994) described the way in which the quantitative relation ships between the data sets representing the deposit recognition criteria and known mineral occurrences is analyzed using a statistical method that uses Bayes' Rule. A series of binary maps is created for mineral occurrences and recognition criteria. The locations of known mineral occurrences are treated as points. Each point, is assumed to have a unit area of 100×100 m (thus the nominal area of a mineral occurrence), is used to rasterize the mineral occurrence and deposit recognition criteria maps. The resulting binary maps are used as input maps to Bayesian statistical analysis and the end product is a sum of weights map ranking favorable areas.

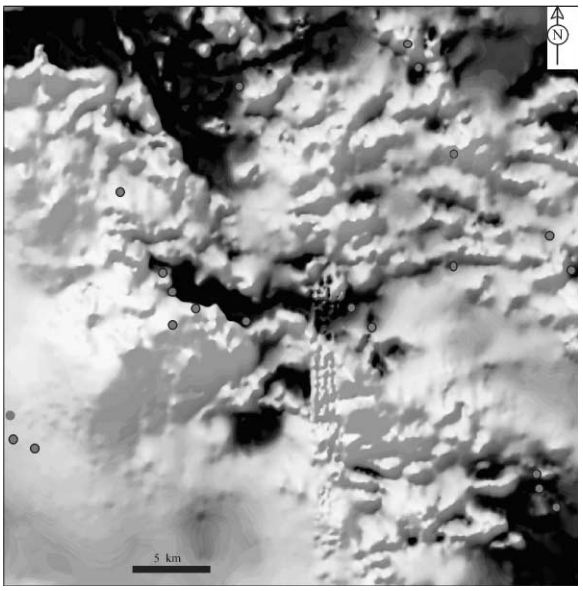

Fig. 4. Shaded relief map of total magnetic intensity.

Each binary map depicts areas where the test domain represented by the map is either present (D_p) or absent (D_n). Scoring is then performed using that domain and known mineral occurrences, in order to obtain a range of positive and negative weights (W^+ and W^-). For details on the mathematical basis for calculating weights refer to Bonham-Carter (1994). Turner (1997) suggested a simplified approach based on an approximation for the weights as follows:

Positive spatial association if:	% mineral occurrences in D_P/% of total area occupied by $D_p > 1$.
Negative spatial association if:	% mineral occurrences in D_P/% of total area occupied by $D_p < 1$.
No spatial association if:	% mineral occurrences in D_P/% of total area occupied by $D_p = 1$.

In the case of positive associations, more known mineral occurrences fall in the test domain (D_P) than would be expected if the mineral occurrences and test domain are unrelated. Conversely, a negative association implies the occurrence of fewer known mineral deposits in the test domain than would be expected if the mineral occurrences and test domain are unrelated.

Since the area covered by a mineral occurrence is much smaller than the domain being considered, an approximation to the true weights-of-evidence are estimated by taking the natural log of the ratios

$$W^+ = \ln(\%\ \text{mineral occurrence in } D_p / \%\ \text{of toal area occupied by } D_p);$$

$$W^- = \ln(\%\ \text{mineral occurrence in } D_n / \%\ \text{of toal area occupied by } D_n).$$

These estimates would be equal to the true W^+ and W^- if the unit area assumed for deposit points is infinitely small (Bonham-Carter, pers. comm., 2000).

These weights give unitless measures of spatial correlation between mineral occurrences and recognition criterion (i.e., test domain). The contrast, $C = W^+ - W^-$, combines these weights into an overall measure of association for a given test domain. For a positive spatial association, C is positive; C is negative in case of negative correlation.

For each test domain the maximum contrast often gives the best measure of spatial correlation with the mineral occurrence points in the case of a large area and a large number of mineral occurrences (Bonham-Carter, 1994; Turner, 1997; Wilkinson et al., 1999). In the case of a small area and a small number of mineral occurrences the uncertainty of the weights could be large and, therefore, C can be meaningless. The Studentized value of C, calculated as the ratio of C to its standard deviation, $C/s(C)$, serves as an approximate

test of the statistical significance of the spatial correlation between the mineral occurrence points and a test domain (Bonham-Carter, 1994). The standard deviation (s) of C is the square root the sum of the variances of the weights

$$s(C) = \sqrt{s^2(W^+) + s^2(W^-)},$$

where expressions for the variances of the weights are given in Bonham-Carter (1994, Chapter 9). The Studentized value of C is used to define the optimum cutoff.

Here we adopt the simplified weight-of-evidence analysis approach as used by Turner (1997) to create a predictive GIS model for exploration for sediment-hosted gold deposits in a large area of north-central Nevada. Turner (1997) simply added the weights for each predictor map together in order to create a ranked-favorability map. Turner (1997) did not convert the sum of the weights to posterior probability, nor did he test the conditional independence of the input recognition criteria binary maps, as explained by Bonham-Carter (1994). This approach, modified by calculating the Studentized value of C as well as by applying the pairwise conditional independence test, is used here for the sediment-hosted gold and base metal deposits of the Takab area, which appear to share several similarities with those of north-central Nevada.

7. Weights-of-evidence analysis

For the Takab area the approach was implemented in a GIS. Four binary maps (test domains), representing the four deposit recognition criteria, were generated with buffer zones at distances of 100–500 m (in increments of 100 m) away from criteria outlines. Weights were calculated at every location (pixel) for each map. The weighted binary maps were combined to create a final predictive map. We show the result on the "sum of the weights" map (e.g., Turner, 1997), and not as a posterior probability map as used by Bonham-Carter et al. (1989) and Bonham-Carter (1994) and others. In terms of order or ranking relationships there is a 1 : 1 correspondence between the "sum of weights" map and posterior probability map (Bonham-Carter, pers. comm., 1999).

7.1. Analysis of host lithologies domain

Favorable host rocks are exposed over 12% of the Takab area. These are buffered in order to include potentially favorable lithologies that may have been covered by unfavorable lithologies. The rasterized mineral occurrence map was digitally overlain with the buffered favorable host lithology map to calculate the weights of evidence (W^+ and W^-) for cumulative distance away from the favorable host lithology (Table 1). The optimum cutoff distance was selected at 300 m away from the outline of the host lithology on the basis that the highest Studentized value of C ($C/s(C) = 4.04$) is estimated at this distance. Twelve out of 19 occurrences, including the two major gold deposits of the area (Zarshuran and Aghdarreh) and the largest lead–zinc mine of the area (Anguran), fall in the host lithology domain with the 300 m buffer zone (Fig. 5). The weights of this favorable domain used for the final model are

$W^+ = 1.15$, if in a favorable host rock domain;

$W^- = -0.77$, if not in a favorable host rock domain.

7.2. Analysis of heat sources domain

Surface exposures of Tertiary igneous rocks and the interpreted high magnetic susceptibility igneous rocks beneath the sediments were combined in a binary raster map to represent the heat sources driving the migration of mineralizing hydrothermal solutions. The resulting heat source domain map was buffered at distances of 100–500 m, and weights of evidence, contrast C, and Studentized value of C were calculated (Table 1). The optimum buffer, yielding the maximum Studentized value of C, was defined at 200 m. The resulting buffered igneous heat source domain constitutes 31.5% of the area, and 13 out of 19 mineral occurrences are present in this domain (Fig. 6). This weights-of-evidence analysis reveals a moderate to strong correlation between the igneous heat sources and mineral occurrences. This spatial affinity is more evident in the Zarshuran mining district in the central part of the area. The weights used in the final model are

$W^+ = 0.78$, if in a favorable heat source domain;

$W^- = -0.77$, if not in a favorable heat source domain.

7.3. Analysis of hydrothermal alteration domain

Iron oxide and hydroxyl hydrothermal alteration occur over 5.2% of the Takab area. In order to have high confidence that iron oxides in the weights-of-evidence analysis resulted from hydrothermal alteration rather than surface weathering, the iron oxides mapped by principal components analysis and those mapped by reduction-to-the-pole technique were crossed, and the overlapping zones extracted for the weights-of-evidence analysis. Argillic hydrothermal alteration and iron oxide hydrothermal alteration were then combined into a new map which was used as the third binary predictor input map for weights-of-evidence analysis. The resulting hydrothermal alteration domain map was buffered at distances of 100–500 m, crossed with the raster mineral

Table 1
Weights of evidence analysis of recognition criteria domains

Distance (m)	Mineral occ. points	% occ.	No. of pixels in domain	% domain	Ratio[a]	W^+	W^-	C[b]	$S^2(W^+)$[c]	$S^2(W^-)$[d]	$S(C)$[e]	$C/s(C)$ [f]
Host lithology domain												
100	8	42.11	26,234	14.70	2.86	1.05	−0.39	1.44	0.13	0.09	0.46	3.10
200	10	52.63	30,805	17.26	3.05	1.11	−0.56	1.67	0.10	0.11	0.46	3.64
300	**12**	**63.16**	**35,828**	**20.07**	**3.15**	**1.15**	**−0.77**	**1.92**	**0.08**	**0.14**	**0.48**	**4.04**
400	12	63.16	40,006	22.42	2.82	0.39	−0.74	1.14	0.08	0.14	0.48	2.39
500	14	63.16	42,874	24.02	2.63	0.97	−0.72	1.69	0.07	0.20	0.52	3.24
Heat source domain												
100	12	63.16	52,300	29.30	2.16	0.77	−0.65	1.42	0.08	0.14	0.48	2.98
200	**13**	**68.42**	**56,200**	**31.49**	**2.17**	**0.78**	**−0.77**	**1.55**	**0.08**	**0.17**	**0.49**	**3.14**
300	13	68.42	75,207	42.14	1.62	0.48	−0.61	1.09	0.08	0.17	0.49	2.21
400	13	68.42	79,358	45.14	1.52	0.39	−0.55	0.94	0.08	0.17	0.49	1.91
500	13	68.42	85,358	47.83	1.43	0.36	−0.50	0.86	0.08	0.17	0.49	1.74
Hydrothermal alteration domain												
100	6	31.58	19,369	10.85	2.91	1.07	−0.26	1.33	0.17	0.08	0.49	2.70
200	9	47.37	27,944	15.66	3.03	1.11	−0.47	1.58	0.11	0.10	0.46	3.44
300	**12**	**63.16**	**36,699**	**20.56**	**3.07**	**1.12**	**−0.77**	**1.89**	**0.08**	**0.14**	**0.48**	**3.97**
400	12	63.16	43,424	24.33	2.60	0.39	−0.72	1.11	0.08	0.14	0.48	2.34
500	13	84.21	45,313	25.39	3.32	1.20	−1.55	2.75	0.08	0.33	0.63	3.55
Structural domain												
100	7	36.84	29,119	16.32	2.26	0.81	−0.28	1.10	0.14	0.08	0.48	2.30
200	**12**	**63.16**	**39,570**	**22.17**	**2.85**	**1.05**	**−0.75**	**1.79**	**0.08**	**0.14**	**0.48**	**3.77**
300	12	63.16	64,977	36.41	1.73	0.55	−0.55	1.10	0.08	0.14	0.48	2.31
400	14	73.68	73,222	41.03	1.80	0.39	−0.81	1.20	0.07	0.20	0.52	2.30
500	15	78.95	81,673	45.76	1.73	0.55	−0.95	1.49	0.07	0.25	0.56	2.65

[a] % occ./% domain.
[b] Contrast.
[c] Variance of W^+.
[d] Variance of W^-.
[e] Standard deviation of contrast.
[f] Studentized value of contrast. Total no. of pixels in the area = 178,476.

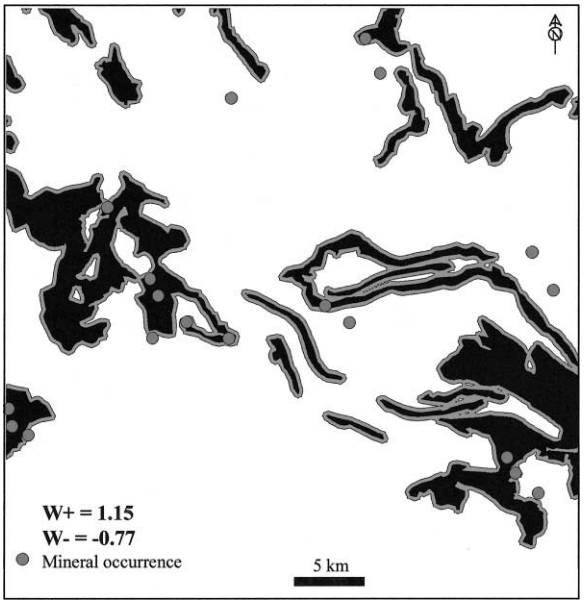

Fig. 5. Host lithology domain (black) with 300 m buffer zones (grey).

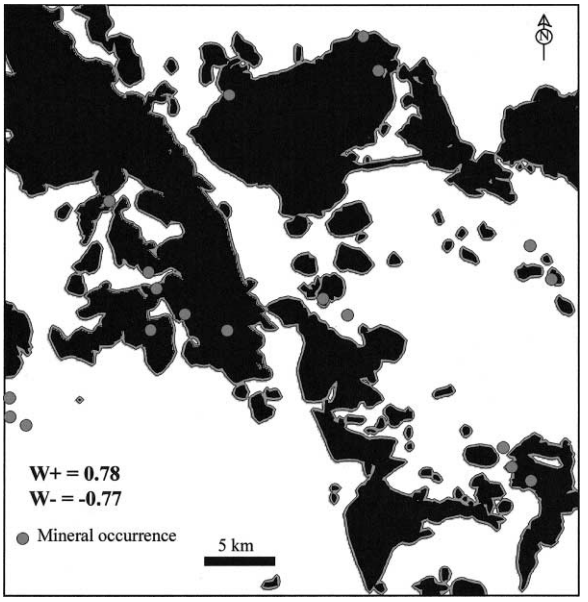

Fig. 6. Igneous heat-source domain (black) with 200 m buffer zones (grey).

occurrence map and weights of evidence, contrast C, and Studentized values of C were calculated (Table 1). The optimum buffer, that yielding the maximum Studentized value of C, was defined at 300 m. The resulting buffered hydrothermal alteration domain covers 20.6% of the study area, and 12 out of 19 mineral occurrences are present in this domain (Fig. 7). The weights of evidence analysis reveals a strong

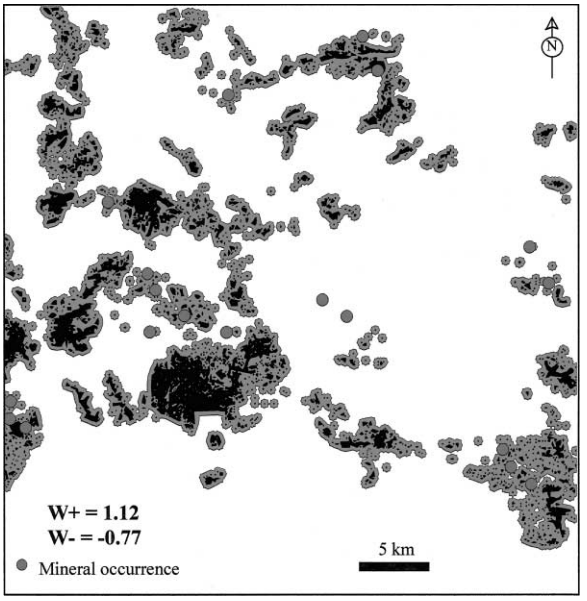

Fig. 7. Hydrothermal alteration domain (black) with 300 m buffer zones (grey).

correlation between the hydrothermal alteration and mineral occurrences (Table 1). The weights used in the final model are

$W^+ = 1.12$, if in a favorable hydrothermal alteration domain;

$W^- = -0.77$, if not in a favorable hydrothermal alteration domain.

7.4. Analysis of structures domain

Known mineralization in the Takab area is associated with linear structures trending NE–SW, E–W and NW–SE. Structures digitized from the geological map were combined with those extracted from the shaded relief image of the total magnetic field. The resulting structural domain was rasterized, buffered at distances of 100–500 m, and crossed with the raster mineral occurrence point map to estimate weights of evidence of the domain (Table 1). The optimum buffer was defined at 200 m. The resulting buffered structural domain covers 22.2% of the area, and 12 out of 19 mineral occurrences are present in this domain (Fig. 8). The weights of evidence analysis reveals a strong correlation between the structural domain and mineral occurrences. The weights used in the final model are

$W^+ = 1.05$, if in a favorable structural domain;

$W^- = -0.75$, if not in a favorable structural domain.

8. Test of conditional independence

We now have four binary predictor maps that can be combined, once the assumption of conditional independence between all pairs of maps with respect to mineral occurrences (Bonham-Carter, 1994) is tested. Conditional independence between all pairs of binary maps is checked to identify the maps that must be used in, or rejected from, the combination procedure. Conditional independence was tested by formulating the null hypothesis of pairwise conditional independence of the predictor binary maps. Then the χ^2 test was run to check if the null hypothesis is rejected at the 95% significance level.

According to Bonham-Carter (1994), Eq. (1) defines the relationship if two binary patterns are conditionally independent with respect to a set of mineral occurrence points:

$$N\{B_1 \cap B_2 \cap D\} = \frac{N\{B_1 \cap D\}N\{B_2 \cap D\}}{N\{D\}}, \quad (1)$$

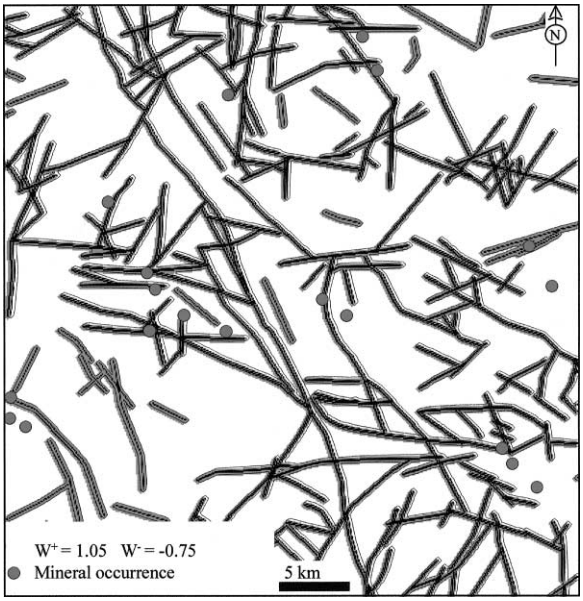

Fig. 8. Structural domain (black) with 200 m buffer zones (grey).

where B_1 and B_2 are two binary predictor maps and D represents mineral occurrences. The left-hand side of the equation is the observed number of deposits occurring in the overlap region where both binary patterns B_1 and B_2 are present. The right-hand side is the predicted number of deposits in this overlap zone. The relationship leads to a contingency table calculation for testing the conditional independence of two binary patterns (Table 2). The four cells in the table correspond to the four possible overlap conditions between two binary patterns where mineral occurrence points are present. The conditional independence is tested by calculating χ^2 as follows:

$$\chi^2 = \sum_{i=1}^{4} \frac{(observed_i - expected_i)^2}{expected_i}. \quad (2)$$

Because the mineral occurrences are considered as points, or single unit cells, the resulting values of χ^2 are unaffected by the units of area measurement. The calculated values can then be compared with standard values of χ^2 to verify if the conditional independence hypothesis holds at 95% probability with one degree of freedom. The χ^2 values for each pair of binary predictor maps for all the four overlap conditions can be calculated using the contingency tables (Bonham-Carter, 1994). A sum of these four χ^2 values gives the total χ^2 value for each possible pair of the binary patterns.

An example of such a contigency table for one pair of binary maps in Takab area, viz., hydrothermal alteration and host lithology, is shown in Table 3. The total χ^2 values for each pair of binary predictor maps are shown in Table 4. The standard χ^2 value with one degree of freedom at the 95% significance level is 3.84 (Davis, 1986). It can be seen from Table 4 that the χ^2 values for all the pairs of binary predictor maps are less than 3.84. Thus, the null hypothesis of conditional independence is not rejected at the 95% significance level for any of the six pairs of maps.

9. Prospectivity model

The predictive exploration model was generated by summing the weights of evidence of four binary

Table 2
Contingency table for testing conditional independence hypothesis. Four values within table are either expected values, assuming conditional independence, which are calculated from marginal totals (Eq. (1)), or observed values measured from maps. There is 1 degree of freedom (adapted from Bonham-Carter, 1994, Chapter 9)

	B_1 present	B_1 absent	Totals
B_2 present	$N\{B_1 \cap B_2 \cap D\}$	$N\{\bar{B}_1 \cap B_2 \cap D\}$	$N\{B_2 \cap D\}$
B_2 absent	$N\{B_1 \cap \bar{B}_2 \cap D\}$	$N\{\bar{B}_1 \cap \bar{B}_2 \cap D\}$	$N\{\bar{B}_2 \cap D\}$
Totals	$N\{B_1 \cap D\}$	$N\{\bar{B}_1 \cap D\}$	$N\{D\}$

Table 3
Example of contingency table for testing conditional independence between pair of binary maps, viz., hydrothermal alteration and host lithology. χ^2 values shown in table are added to yield total χ^2 value shown in Table 4

	Host lithology present			Host lithology absent			Totals
	Observed	Expected	χ^2	Observed	Expected	χ^2	
Hydrothermal alteration present	6	7.58	0.33	6	4.42	0.56	12
Hydrothermal alteration absent	6	4.42	0.56	1	2.58	0.97	7
Totals	12	12	0.89	7	7	1.53	19

Table 4
Total χ^2 values for all six pairs of binary maps

Binary map	Heat sources	Hydrothermal alteration	Lineaments
Host lithology	0.07	2.42	1.93
Heat sources		1.54	1.12
Hydrothermal alteration			0.33

Table 5
Summary of weights-of-evidence for deposit recognition criteria binary maps

Recognition criteria	W^+	W^-
Favorable host lithology	1.15	−0.77
Igneous heat sources	0.78	−0.77
Hydrothermal alteration domain	1.12	−0.77
Favorable structural domain	1.05	−0.75
Cumulative total	**4.10**	**−3.06**

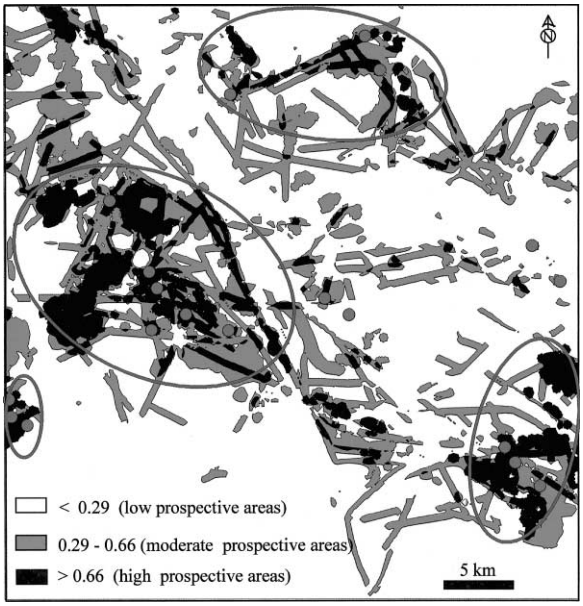

Fig. 9. Predictive model map outlining prospective mineralized zones in Takab area.

maps representing the epithermal gold and base metal recognition criteria. The various overlap combinations of the binary maps result in the highest cumulative weights for the locations where all the recognition criteria are present. The lowest weights are located where favorable conditions are scarce. The predictive weights range from a maximum of 4.10 to a minimum of −3.06, providing a relative measure for prioritizing areas of exploration potential (Table 5).

Based on the coincidence of the ranked criteria, the resulting predictive map was classified into three categories: low prospectivity, moderate prospectivity and high prospectivity (Fig. 9). The threshold between low prospectivity and moderate prospectivity zones is set by $W_1^+ + W_2^+ + W_1^- + W_2^-$, where subscripts refer to the domains with the two lowest weights, thus, $+0.78 + 1.05 + (-0.77) + (-0.77) = +0.29$. The threshold between the moderate prospectivity and high prospectivity zones is set by a corresponding calculation based on the domains with the three lowest weights, thus $+0.78 + 1.05 + 1.12 + (-0.77) + (-0.77) + (-0.75) = +0.66$.

The prospectivity model (Fig. 9) places 16 of 19 (84%) of the known mineral deposits of the Takab area (including all the major gold deposits and base metal mines) in the high prospectivity zone, which represents 8.5% of the total area. The model places four important mining districts in the high prospectivity zone, namely Zarshuran in the central part, Aghdarreh in the southwest, Anguran in the southeast and Biche-Bagh in the northeast. In addition, the model suggests as highly prospective some areas not previously recognized as favorable in the northwest of the Takab area, the central-south part between the Zarshuran and Anguran mining districts, and some small areas in the western part. These require follow-up investigations.

10. Conclusions

This paper demonstrates that successful development of a GIS model for epithermal gold and base metal reconnaissance in a rugged terrain and difficult in access, such as Takab, requires:

1. investigation of the genetic concepts of particular mineral deposit(s) and recognition of the spatial features (deposit recognition criteria) that control the known mineralizations;
2. analysis of cost-effective remotely-sensed data for a fast detection of the spectral and magnetic signatures of deposit recognition criteria; and
3. application of weights-of-evidence methodology, within a GIS framework, to quantify the spatial correlations between the deposit recognition criteria and the known mineral occurrences and to predict prospective areas.

References

Alavi, M., 1993. Tectonics of the Zagros orogenic belt of Iran: new data and interpretations. Tectonophysics 229, 211–238.

Alavi, M., Hajian, J., Amidi, M., Bolourchi, H., 1982. Geology of Takab–Shahin–Dez Quadrangle. The Ministry of Mines and Metals of Iran, Tehran, 100pp.

Asadi, H.H., Carranza, E.J.M., Hale M., 1998. GIS and remote sensing for epithermal gold exploration in northwest Iran. Proceedings of International Conference on GIS for Earth Science Applications, Ljublijana, Slovenia, 17–22 May 1998, pp. 57–73.

Asadi, H.H., Hale, M., 1999a. Integrated analysis of aeromagnetic, Landsat TM and mineral occurrence data for epithermal gold exploration in northwest Iran. Proceedings of the 13th International Conference on Applied Geologic Remote Sensing, Vancouver, British Columbia, Canada, 1–3 March, p. 8.

Asadi, H.H., Hale, M., 1999b. Magmatic contribution to the Carlin-type gold deposit at Zarshuran, Iran. Proceedings of the Fifth joint SGA-IAGOD International Meeting, Imperial College, London, p. 4 .

Asadi, H.H., Voncken, J.H.L. Hale, M., Kuhnel, R.A., 1999a. Petrography, mineralogy and geochemistry of the Zarshuran Carlin-like gold deposit. Mineralium Deposita, in press.

Asadi, H.H., Voncken, J.H.L., Hale, M. 1999b. Invisible gold at Zarshuran, Iran. Economic Geology, in press.

Bagby, W.C., Berger, B.R., 1985. Geologic characteristics of sediment-hosted, disseminated preceous metal deposits in the western United States. In: Berger, B.R., Bethke, P.M. (Eds.), Geology and Geochemistry of Epithermal Systems, Reviews in Economic Geology, 2. Society of Economic Geology, pp. 169–202.

Bariand, P., 1962. Contibution a' la mineralogie de l' Iran. Ph.D. Dissertation, Université de Paris, Faculté des Sciences, Ser. A. No. 980.

Berberian, M., King, G.C.P., 1981. Toward a paleogeography and tectonic evolution of Iran. Canadian Journal of Earth Sciences 18, 210–265.

Bonham-Carter, G.F., 1994. Geographic Information Systems for Geoscientists, Modelling with GIS. Pergamon, Oxford, 398pp.

Bonham-Carter, G.F., Agterberg, F.P., Wright, D.F., 1989. Weights-of-evidence modelling: a new approach to mapping mineral potential. In: Agterberg, F.P., Bonham-Carter, G.F. (Eds.), Statistical Applications in the Earth Sciences. Geological Survey of Canada, Paper 89–9, pp. 171–183.

Daliran, F., Walteher, J., Stuben, D., 1999. Sediment-hosted disseminated gold mineralization in the northTakab geothermal field, NW Iran. Proceedings of the Fifth joint SGA-IAGOD international meeting, Imperial College, London, p. 4.

Davis, J.C., 1986. Statistics and Data Analysis in Geology, 4th Edn. Wiley, New York, 641pp.

Geological Survey of Iran, 1998. Geological map of Takab area (1 : 100,000 scale), Tehran.

Karimi, M., 1992. Geology, petrography, and mineralogical studies of Zarshuran gold deposit. Internal Report, Kansaran Engineering Consultant, Tehran, 250pp (in Persian).

Mineral Export Company, 1995. Geological map of the Agh-Darreh deposit (1 : 5,000 scale), Tehran.

Ministry of Mines and Metals of Iran, 1994. Mineral deposits of Takab area. Internal report, Tehran, 275pp (in Persian).

Mohajer, Gh., Parsaie, H., Fallah, N., Ma'dani, F., 1989. Mercury exploration in the Saein Dez-Takab area. Ministry of Mines and Metals of Iran, Tehran, 227pp (in Persian).

Paterson, N.R., Reeves, C.V., 1985. Applications of gravity and magnetic surveys: the state-of-the-art in 1985. Geophysics 50, 2558–2594.

Samimi, M., 1992. Reconnaissance and preliminary exploration in the Zarshuran area. Report, Kavoshgaran Engineering Consultant, Tehran, 47pp (in Persian).

Turner, D.D. 1997. Predictive GIS model for sediment-hosted gold deposits, north-central Nevada, U.S.A. Proceedings of Exploration 97: Fourth Decennial International Conference on Mineral Exploration, pp. 115–126.

Wilkinson, L., Harris, J., Kjarsgaard, B., 1999. Searching for kimberlite: preliminary weights-of-evidence modeling of the Lac De Gras area, NWT, using GIS technology. Proceedings of the 13th International Conference on Applied Geologic Remote Sensing. Vancouver, Vol. 1, 263–271.

Zanjani, A., 1945. Biche-Bagh copper mine. Internal Report, Ministry of Mines and Metals of Iran, Tehran, 15pp (in Persian).